Retrieval of Arctic Sea Ice Parameters by Satellite Passive Microwave Sensors: A Comparison of Eleven Sea Ice Concentration Algorithms

Natalia Ivanova, Ola M. Johannessen, Leif Toudal Pedersen, *Member, IEEE*, and Rasmus T. Tonboe

***Abstract*—Eleven algorithms for the passive-microwave measurement of sea-ice were implemented and inter-compared. Daily, monthly and annual Arctic sea-ice concentration, area and extent were calculated by the algorithms using daily microwave brightness temperatures from SMMR, SSM/I, and SSMIS for the period 1979–2012. The differences between the 11 sea-ice concentration estimates—structural uncertainties—were quantified and analyzed spatially and seasonally. The algorithms differ in annual sea-ice area by 0.0–1.3 million km^2 and in extent by 0.0–0.6 million km^2. Linear trends for 34- and 21-year periods were calculated and compared for sea-ice concentration, area and extent. Low-frequency algorithms obtained annual Arctic sea-ice area decrease of 0.534–0.573 million km^2 per decade (0.439–0.491 million km^2 per decade for the extent) over the period 1979 to 2012, and a decrease of 0.866–0.975 million km^2 per decade (0.767–0.812 million km^2 per decade for the extent) for the 1992–2012 period. High-frequency algorithms obtained a decrease of 0.766–0.978 million km^2 per decade in the area and 0.758–0.814 million km^2 per decade in the extent over the period 1992–2012. Results for all the algorithms have close agreement on the strength of the negative trend in Arctic sea-ice area and extent, but are individually biased from the mean. The algorithms' ensemble mean and standard deviation in sea-ice concentration, describing part of the uncertainty, are presented to provide users with more insight into the uncertainties and potential biases of sea-ice concentration data.**

***Index Terms*—Algorithms, arctic regions, microwave radiometry, remote sensing, sea ice concentration.**

I. Introduction

THE sea-ice cover in the Arctic is shrinking and the ice is thinning leading to an acceleration of global climate change [40]. The spatio-temporal record of satellite passive microwave measurements shows that during the last three decades the average September sea-ice extent (the area within the ice-ocean margin which is defined by 15% sea-ice concentration) has decreased with an average rate of almost 0.8 million km^2 per decade [10]. It is therefore of particular importance to be able to retrieve sea-ice parameters accurately and with known uncertainties for accurate assessment of climate-change and assimilation of sea-ice in models for future climate projections. However, well-known Internet resources disagree on the absolute values of near-real-time sea-ice parameters. Examples of operational sea-ice extent data for September and March are shown in Table I for the retrievals from: the NORSEX algorithm (Norwegian Remote Sensing Experiment in a Marginal Ice Zone) [34] at Arctic Regional Ocean Observing System—Arctic ROOS (http://arctic-roos.org); the NASA Team algorithm [7] at the National Snow and Ice Data Center—NSIDC (http://nsidc.org); the ASI algorithm [21] at the Institute of Environmental Physics (IUP), University of Bremen (http://iup.physik.uni-bremen.de); and a combination of the algorithms Bristol [37] and Bootstrap frequency mode [11] at EUMETSAT Ocean and Sea Ice Satellite Application Facility—OSI SAF (http://osisaf.met.no, http://ocean.dmi.dk/arctic/icecover.uk.php). While the NSIDC and the IUP show similar results, there can be larger differences, such as between Arctic ROOS and OSI SAF in March (0.7 million km^2) and between Arctic ROOS and the IUP in September (0.9 million km^2). Differences in the annual Arctic sea-ice area (the area of ice-covered ocean where there is at least 15% sea ice) can reach up to 1 million km^2 (the maximum difference between a pair of algorithms during 1979–2008, 8 algorithms considered) [20].

TABLE I
SEA-ICE DATA SOURCES

Source (Algorithm)	March 2012	September 2012
Arctic ROOS (NORSEX)	14.9 (19.03)	4.2 (15.09)
NSIDC (NASA Team)	15.2 (18.03)	3.4 (16.09)
IUP (ASI)	15.3[a](21.03)	3.3[b] (14.09)
OSI SAF (Bristol + Bootstrap F)	15.6 (15.03)	3.9 (14.09)

Minimum and maximum sea-ice extent in 2012 obtained with SSM/I input data, in million km^2. The date of the event is shown in parentheses with $\pm(2-3)$-day accuracy.
[a] SSMIS-based data adapted to the AMSR-E time series.
[b] AMSR2-based data adapted to the AMSR-E time series.

The large variety of algorithms available and the apparent differences between them constitute the motivation for this research. In addition, the validation of the algorithms is a

Manuscript received March 21, 2013; revised October 7, 2013 and February 10, 2014; accepted February 27, 2014. Date of publication April 3, 2014. This work was funded by the Research Council of Norway through the project ArcticSIV (contract no. 207584), the Nansen Environmental and Remote Sensing Center through the Trond Mohn donation, and the ESA/ESRIN (Sea Ice-CCI) through the sea ice project (contract no. 4000104733/11/I-AM). The work was also supported by the Danish Agency for Science, Technology and Innovation and is a part of the Greenland Climate Research Centre.

N. Ivanova is with the Nansen Environmental and Remote Sensing Center, 5006 Bergen, Norway (e-mail: natalia.ivanova@nersc.no).

O. M. Johannessen is with the Nansen Environmental and Remote Sensing Center, 5006 Bergen, Norway and Nansen Scientific Society, Bergen, Norway (e-mail: ola.johannessen@nersc.no).

L. T. Pedersen and R. T. Tonboe are with the Danish Meteorological Institute, 2100 Copenhagen, Denmark (e-mail: ltp@dmi.dk; rtt@dmi.dk).

Digital Object Identifier 10.1109/TGRS.2014.2310136

TABLE II
SEA-ICE ALGORITHMS

Name	Reference	Channels	Res	A. Input	Based on
NORSEX	[41]	19V, 37V	25	SATclim	Simplified RTE
NASA Team	[7]	19V, 19H, 37V	25		PR, GR
UMass-AES	[43]	19V, 37V	25		Linear combination of TBs
Bootstrap	[11]	19V, 37V, 37H	25		Cluster analysis of emissivity scatter plots: polarization and frequency mode
Near 90GHz	[42]	85V, 85H	12.5		P
Cal Val	[34]	19V, 37V	25		Linear combination of TBs
Bristol	[37]	19V, 37V, 37H	25	SATclim	Same as Bootstrap but the two modes combined
NORSEX-85H	[25]	19V, 37V, 85H	12.5	SATclim	NORSEX, higher resolution by using 85H
TUD	[32]	19V, 37V, 37H, 85V, 85H	12.5		Bootstrap, P
NASA Team 2	[28]	19V, 19H, 37V, 85V, 85H	12.5	Mod. atm.	PR, rotated in certain domains
ASI	[21]	85V, 85H	12.5		Near 90GHz, Bootstrap

Res – resolution in km, A. Input – additional input, V - vertical and H - horizontal polarizations, SATclim – surface air temperature (climatology), RTE – radiative transfer equation, Mod. atm – modeled atmospheres, PR - polarization ratio, GR – gradient ratio, P – polarization, TBs – brightness temperatures.

challenge due to the lack of validation data. Validation data are sparse because of the severe weather and ice conditions in the Arctic, which complicate direct in situ measurements and the long periods of darkness and cloudiness, which limit satellite measurements in the visible range. The main objectives of this study are to compare and analyze sea-ice retrievals from the different algorithms and to quantify the differences. The research builds and expands upon several previous algorithm comparison works. Comparisons of Bootstrap and NASA Team algorithms were done by [17] for 1989 and by [13] for 1992 and showed differences in Arctic sea-ice concentrations of -8% to $+10\%$ and -7% to $+7\%$, respectively. The discrepancy between the algorithms is caused by differences in: 1) choice and utilization of the channels (frequency and polarization), 2) tie-points and their adjustments, 3) sensitivities to changes in physical temperature of the surface, and 4) weather filters [13]. Nine algorithms—NORSEX, NASA Team, Bootstrap (considered as two algorithms according to its modes), Near 90, Cal Val, Bristol, TUD, and NASA Team2—were intercompared [2] in terms of their sensitivity to atmospheric effects. Algorithms using high frequencies such as Near 90, TUD, and NASA Team2 were found to be more sensitive to the atmospheric effects over open water. It was also found that algorithms using 19 V and 37 V channels (Bootstrap frequency mode, CalVal, and NORSEX) were least sensitive to cloud liquid water and wind. The algorithms that also use 19 H and/or 37 H channels (Bristol and NASA Team) are more sensitive to wind and clouds over open water [2]. We will use the term "low-frequency" in application to algorithms using frequencies up to 37 GHz. The algorithms using the high-frequency channels (85.5/91.7 GHz) will be referred to as "high-frequency algorithms," although some of them also include low-frequency channels (NASA Team2, NORSEX-85 H, and TUD). Seven algorithms were compared in [4]: NASA Team, Bootstrap (two modes), Near 90, Bristol, TUD, and NASA Team2 for the cold period (31 October–31 March) of the years 2000–2004. Only areas where the concentration is near 100% were considered. Average sea-ice concentration for the cold period varied from 96% to 100% depending on the algorithm used. NASA Team2 (the only algorithm having a built-in cutoff at 100%) showed the lowest standard deviation of 1.7% for the mean concentration value of 98.9%. Among the unconstrained algorithms (allowing sea ice concentrations below 0% and above 100%), the lowest standard deviation of 3% (for the mean concentration value of 101.7%) was found for the TUD algorithm.

We consider structural uncertainty, which is a term describing the bias relative to a true reference caused by the use of different methodologies or algorithms. Since the true value is not known, we perform this evaluation with the average of all algorithms as the reference. Our work is unique in its consistent inter-comparison of 11 sea ice algorithms (Table II) and quantification of differences between them covering the entire Arctic, all seasons and the longest time period of multichannel passive microwave data (1979–2012). The inter-comparison covers both spatial (concentrations) and temporal (area and extent) aspects of the algorithm retrievals. Knowledge of the algorithms uncertainty plays an important role in future Arctic sea ice projections [22].

In Section II a description of the input data is given, in Section III the 11 sea ice algorithms and implementation issues are described. The next two sections present an analysis of the differences between the algorithms in sea-ice area, extent (Section IV) and concentration (Section V). Section VI describes differences in the linear trends in area, extent and concentration as obtained by the algorithms. Finally, Section VII provides discussion and conclusions.

II. DATA

The input data used in this study are the NIMBUS-7 SMMR (Scanning Multichannel Microwave Radiometer) brightness temperature grids for the Northern Hemisphere for the time period from January 1, 1979 to July 31, 1987 [31] and DMSP SSM/I (Special Sensor Microwave Imager) Daily Polar Gridded Brightness Temperatures for the period from August 1, 1987 to December 31, 2012 [29]. Both of the gridded data sets were

TABLE III
FREQUENCIES AND FOOTPRINTS

SMMR		SSM/I and SSMIS	
Frequency, GHz	Footprint, km^2	Frequency, GHz	Footprint, km^2
18.0	55*41	19.3	70*45
21.0	46*30	22.2	60*40
37.0	27*18	37.0	38*30
		85.5	16*14
		SSMIS	
		91.7	16*13

SMMR [31], SSM/I and SSMIS [29]

obtained [29], [31] from swath data by a simple sum-and-average mapping ("drop-in-the-bucket") to a polar stereographic grid. The grid size for both instruments is 25 km^2 for the low-frequency channels and 12.5 km^2 for the high-frequency channels (only SSM/I and SSMIS). However, the sensor footprint is larger and differs from channel to channel (Table III). The SMMR radiances of the 18, and 37 GHz channels are corrected for instrument drift and sensitivity variations with ecliptic angle [31]. They are also adjusted to correspond more closely to modeled oceanic radiances and those from the DMSP SSM/I [18]. SSM/I data from the F8 DMSP were used for the period from August 1, 1987 to December 2, 1991; the F11 December 3, 1991 to May 2, 1995; F13 from May 3, 1995 to December 13, 2006; F17 (SSMIS) from December 14, 2006 to December 31, 2012. Data were acquired only every other day during the SMMR period, so to be consistent we sample SSM/I data in the same way. Note that the difference between every-day and every-other-day data sets for SSM/I leads to difference in monthly and annual sea-ice area of not more than 0.015 million km^2. It should be noted that the sensors may have different frequencies in the same channel, for example the F17 SSMIS has 91 GHz whereas the F11 and F13 SSMI have 85 GHz in the high frequency channels (see Table III for other channels). This and aforementioned differences in footprint may have consequences for the algorithms outputs.

III. ELEVEN SEA-ICE ALGORITHMS

The algorithms for retrieving sea-ice parameters from satellite passive microwave data used in our paper are presented in Table II with listed references, channels, resolution, additional input and algorithm principle. This table provides a summary background for the reasons of the differences in sea-ice retrievals by the algorithms.

The algorithms employ combinations of brightness temperatures (TB) in different channels (f—frequency, p—polarization) to distinguish open water, first-year ice and multi-year ice. The 19 V and 37 V channels are used in almost all the algorithms because of the large difference in the emissivity between water and ice in the 19 V channel, and between first-year and multi-year ice in the 37 V channel. The horizontal channels can be influenced by layering in the snow [41]; however [7] claims that variability of the H-channels differs from that of the V-channels by only 1 K, which allows using these channels anyway. Polarization ratio [(1)] is another characteristic used to distinguish surface types (in the NASA Team algorithm) because it is small for either ice type compared to that of the ocean

$$PR(f,p_v,p_h)=\frac{TB(f,p_v)-TB(f,p_h)}{TB(f,p_v)+TB(f,p_h)} \tag{1}$$

$$GR(f_1,f_2,p)=\frac{TB(f_2,p)-TB(f_1,p)}{TB(f_2,p)+TB(f_1,p)} \tag{2}$$

$$P(f,p_v,p_h)=TB(f,p_v)-TB(f,p_h). \tag{3}$$

Gradient ratio [(2)], also used in the NASA Team algorithm, allows distinguishing first-year and multiyear ice types because the brightness temperature difference between the two ice types increases with increasing frequency. The advantage of using brightness temperature ratios is that they are less sensitive to physical temperature variations of the emitting layer of ice/snow. Polarization difference [(3)] for high frequencies, being larger for water than for ice, is used to distinguish these two surfaces in the near 90 GHz algorithms.

We test all the algorithms in similar conditions: input data, weather filters and land-ocean spillover masks. It is noted that the primary scope is to compare variability and spatial/temporal differences, which are relatively independent of the absolute level of ice concentration.

Input Data

The algorithms were applied to the aforementioned every-other-day brightness temperature grids. The low-frequency algorithms cover the period 1979–2012, while the high-frequency algorithms were run for 1992–2012. The high-frequency channels are available from 1987 but we discard data prior to 1992 because of large data gaps in these channels before 1992. To match SMMR and SSM/I satellites the method of [14] was applied to the brightness temperatures and used in all the low-frequency algorithms except NASA Team because it does the match-up by using individual tie-points for each instrument. All the other algorithms use the same tie-points for both SMMR and SSM/I. The adjusted SMMR brightness temperature was defined as

$$TB_{SMMRadjusted}=a\cdot TB_{SMMR}+b. \tag{4}$$

The a and b coefficients have the following values (each marked by the frequency and polarization): $\mathrm{a18v}=0.974$, $\mathrm{b18v}=17.2$, $\mathrm{a18h}=1.023$, $\mathrm{b18h}=8.4$, $\mathrm{a37v}=1.109$, $\mathrm{b37v}=-20.6$, $\mathrm{a37h}=1.149$, and $\mathrm{b37h}=-21.8$ (the values are rounded; please see [5] for full numbers). We obtained these coefficients from scatter plots of the SMMR brightness temperatures in each channel versus those of SSM/I for the period of overlap for these two instruments (July 9 to August 20, 1987).

Weather Filters

Since the radiometer measurements are sensitive to surface and atmospheric variability in channels other than those used for the sea ice algorithms, these additional channels have been used to develop filters that allow screening for strong atmospheric influence. Weather filters are applied to remove false indication of sea ice over open water, caused by atmospheric water vapour, cloud liquid water, and wind roughening of the sea surface [8].

TABLE IV
TIE-POINTS (BRIGHTNESS TEMPERATURES OF OPEN WATER, FYI, AND MYI), SELECTED ALGORITHMS, IN K

Tie-point	Month	Channel	Bristol	NASA Team	NORSEX	UMass-AES
Open Water	March	19V	179.5	185.2	168.9	155.6
		19H		114.4		
		37V	204.0	205.2	193.7	196.6
		37H	141.4			
	September	19V	182.2	185.2	168.9	155.6
		19H		114.4		
		37V	204.0	205.2	193.7	196.6
		37H	144.2			
First-Year Ice	March	19V	248.9	251.2	254.1	239.0*
		19H		235.4		
		37V	238.4	241.1	254.1	244.2*
		37H	230.6			
	September	19V	238.0	251.2	262.3	246.6*
		19H		235.4		
		37V	238.0	241.1	262.3	252.0*
		37H	210.9			
Multi-Year Ice	March	19V	220.1	222.4	214.8	225.8*
		19H		198.6		
		37V	186.0	186.2	193.9	199.6*
		37H	172.9			
	September	19V	219.0	222.4	221.7	233.1*
		19H		198.6		
		37V	192.0	186.2	200.1	206.0*
		37H	178.5			

SAT_{March} = 247 K, $SAT_{September}$ = 268 K; T_{water} =272 K (273 K for UMass-AES), T_{ice} =0.4*SAT+0.6*T_{water};
* - the values are obtained for the table using given SAT, but in the algorithm only emissivities are used.

The same weather filters were applied for all the algorithms: [19] for SMMR and [8] for SSM/I and SSMIS. These filters are based on thresholds for two gradient ratios [(2)]: 1) 37 V and 19 V channels to reduce the effect of wind roughening, cloud liquid water and rain, and 2) 22 V and 19 V channels (SSM/I and SSMIS only) to reduce the water vapor influence and to minimize the effect of ice temperature variations at the ice edge [9]. The weather filters set sea ice concentration C to zero if

$$GR(37\text{ V}/18\text{ V}) > 0.07 \quad (SMMR) \tag{5}$$

$$GR(37\text{ V}/19\text{ V}) > 0.05 \quad \text{and/or}$$

$$GR(22\text{ V}/19\text{ V}) > 0.045 \quad (SSM/I\ and\ SSMIS). \tag{6}$$

Open ocean masks [NSIDC, climatology for 1979–2007] were applied to remove the residual false sea ice indications from the areas that are very unlikely to have ice.

It should be noted that SMMR has 18 GHz channel whereas SSM/I (SSMIS) has 19.35 GHz (Table III), which makes the weather filters work differently with SMMR and SSM/I (SSMIS). Therefore, the weather filter may introduce offsets even if the tie-points for the algorithm are adjusted.

Land-Ocean Spillover Masks

Due to the coarse footprint of the instruments (see Table III for more details), false sea ice indications may appear along the coastlines (the brightness temperature of ice and land are much higher than that of water). Therefore, land-ocean spillover masks [9] were applied to outputs from all the algorithms.

We choose to implement the algorithms according to their published versions (Table II) and therefore we also use the original tie-points with every algorithm (see Table IV for selected examples of tie-points sets). However, in cases when tie-points for a certain algorithm have been updated after the original publication (ASI, NASA Team, and Bootstrap algorithms) we use the updated version. The Bristol algorithm lacks the exact tie-points values in the publication, and therefore we applied the set published in [1]. This set was chosen because [36] emphasize the importance of seasonal tie-points being used in this algorithm. The Near 90 GHz algorithm defines its tie-points for every swath [42], but in our work we defined it for every daily grid. To define the areas of ice and water for sampling the tie-points, we used retrievals from another high-frequency algorithm, ASI. It was chosen out of 4 other high-frequency algorithms because it does not include any information from the low-frequency channels. The sea ice tie-point is calculated as the average polarization difference for all the pixels where ASI shows 100% sea ice concentration, and the open water tie-point is taken from the grid cells where ASI gives 0% sea ice concentration (before the weather filter is applied). Our implementation of the ASI algorithm differs from the original paper [21], where it is suggested to set the concentration to zero when the NASA Team retrieval shows less than 30% concentration. Instead, we set to zero only the grid cells where the Bootstrap algorithm gives zero [38].

The instruments SMMR and SSM/I (SSMIS) do not observe the area around the North Pole (611 km in radius for SMMR and 311 km for SSM/I and SSMIS) due to the orbit inclination [NSIDC], and we assume the sea ice concentration to be 100% in these areas. The fact that this area is larger for SMMR than for SSM/I (SSMIS) means that the overestimation of the sea ice area by the algorithms during the SMMR period will be larger than for SSM/I (SSMIS), assuming the amount of melt-ponds is the same every summer.

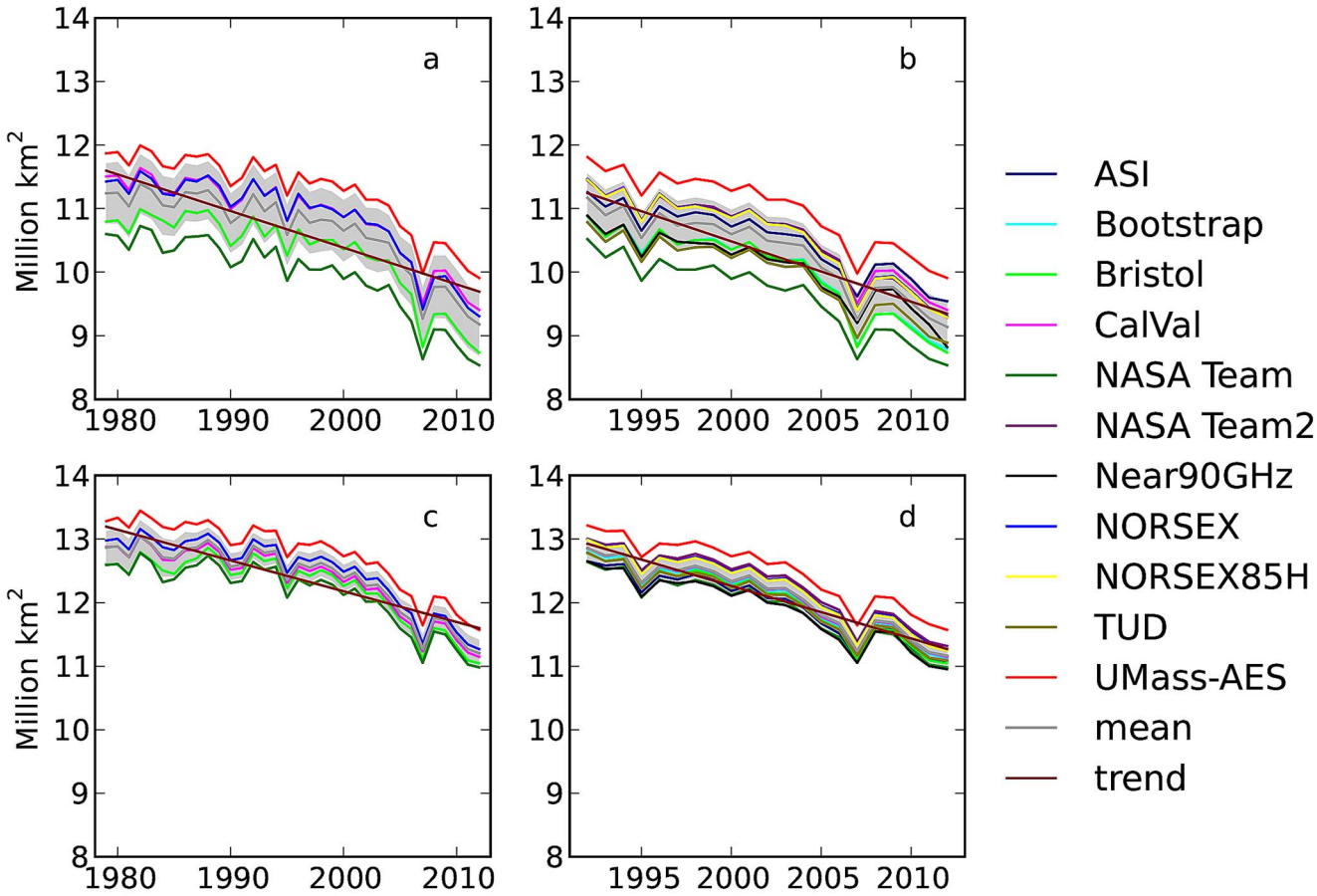

Fig. 1. Annual Arctic sea-ice area (top row) and extent (bottow row) obtained by the five low-frequency algorithms (Bootstrap is not included) for the period 1979–2012 (Left column) and all the 11 algorithms (both low- and high-frequency) for the period 1992–2012 (Right column) with the average (gray line) and shading which marks the standard deviations (std) of all algorithms from the ensemble mean for each year. The ensemble mean trend line is dark red.

As was mentioned in the Introduction, the results from algorithms ASI, Bootstrap, Bristol, NASA Team, and NORSEX are published in the web-sources. However, our retrievals obtained by the same algorithms differ slightly from these. For the ASI the discrepancy is caused by the fact that we use SSM/I and SSMIS input data, while the original version of the data is for AMSR-E. Also, the thresholds in the weather filter we use [8] are slightly different from the ones used in this web-source [38]. The retrievals from the NASA Team and Bootstrap algorithms presented here differ from the ones published at NSIDC because we did not apply a correction of residual weather-related effects (based on monthly climatological sea surface temperatures) or perform manual corrections to remove spurious ice as was done at NSIDC [9]. In addition, in our work we do not include the Baltic Sea, the Great Lakes, and the Lake Baykal. The results from the NORSEX algorithm presented in this work (and using standard brightness temperatures as input) differ from the version published on Arctic ROOS [5], where near-real-time brightness temperatures were used. The standard data are daily gridded brightness temperature data, which have undergone full calibration, correction and quality assessment [29]. Another reason for disagreement in the NORSEX versions is difference in the post-processing routines such as land-ocean spillover and open ocean masks. The Arctic ROOS NORSEX applies its own masks, while we chose to use better-documented masks from NSIDC (see above). As for the OSI SAF product, we cannot compare our retrievals to it because we consider Bootstrap and Bristol algorithms separately. Our purpose was to perform the algorithm comparison using the same pre- and post-processing routines and auxiliary data for all algorithms to prevent differences in these factors from overshadowing the results.

Four newer algorithms not listed in the Table II should be mentioned: SEALION [23], [24], ECICE [35], Kongoli [26], and IOMASA [30]. They represent a different class of sea-ice concentration algorithms due to their complexity (e.g., using additional inputs from models and other satellite data than passive microwave) and thus are not included in this analysis.

IV. Sea-Ice Area and Extent

Arctic sea-ice area and extent (using a 15% cutoff in concentration) were calculated from sea-ice concentrations obtained by each of the algorithms (Table II). Annual mean sea-ice area and extent are shown in Fig. 1 for 1979–2012 [(a) and (c)] and 1992–2012 [(b) and (d)]. The Bootstrap algorithm showed inconsistency with the other algorithms' behavior for SMMR, which has also influence on the trends assessments. This inconsistency is explained by the fact that original version of the algorithm is meant to use tie-points adjusted to the SMMR brightness temperatures that are matched-up with the SSM/I-AMSR time series [14]. In our research we use the original

TABLE V
(a) CORRELATION TABLE: AREA AND EXTENT 1979–2012. (b) CORRELATION TABLE: AREA AND EXTENT 1992–2012

(a)

		Area				
E		UMass-AES	NORSEX	Cal Val	Bristol	NASA Team
x	UMass-AES	**1.00**	0.98	0.99	0.99	0.95
t	NORSEX	0.99	**1.00**	0.99	0.99	0.96
e	Cal Val	0.99	1.00	**1.00**	1.00	0.97
n	Bristol	0.98	0.99	0.99	**1.00**	0.97
t	NASA Team	0.97	0.98	0.99	0.99	**1.00**

The correlation coefficients here and in the Table VB are calculated from monthly anomalies of area and extent for each algorithm. The upper right half of the matrix is presented by correlation coefficients in area and bottom left – by those in extent.

(b)

		Area									
		ASI	TUD	Near90 GHz	NORSEX 85H	UMass -AES	NORSEX	Cal Val	Bristol	NASA Team2	Bootstrap	NASA Team
	ASI	**1.00**	0.99	0.97	0.96	0.98	0.96	0.97	0.98	0.95	0.94	0.95
	TUD	1.00	**1.00**	0.97	0.97	0.98	0.97	0.98	0.98	0.97	0.98	0.97
E	Near90GHz	0.98	0.98	**1.00**	0.95	0.96	0.95	0.96	0.97	0.94	0.92	0.94
x	NORSEX85H	0.99	1.00	0.98	**1.00**	0.99	1.00	0.99	0.99	0.99	0.96	0.96
t	UMass-AES	0.98	0.99	0.97	0.99	**1.00**	0.99	0.99	0.99	0.98	0.95	0.95
e	NORSEX	0.99	1.00	0.98	1.00	0.99	**1.00**	0.99	0.99	0.99	0.96	0.96
n	Cal Val	0.99	1.00	0.98	1.00	0.99	1.00	**1.00**	1.00	0.99	0.95	0.96
t	Bristol	0.99	1.00	0.99	1.00	0.99	1.00	1.00	**1.00**	0.98	0.95	0.96
	NASA Team2	0.99	0.99	0.98	1.00	0.99	1.00	1.00	0.99	**1.00**	0.96	0.97
	Bootstrap	0.99	1.00	0.98	1.00	0.99	1.00	1.00	1.00	0.99	**1.00**	0.97
	NASA Team	0.99	0.99	0.98	0.99	0.98	0.99	0.99	1.00	0.99	1.00	**1.00**

tie-points, but our match-up coefficients for SMMR (which worked well for all the other algorithms) are different, because we do not use AMSR, but only SMMR-SSM/I. Therefore, the Bootstrap algorithm was excluded from our analysis for the time period of 1979–2012.

The mean difference between the algorithms in annual sea-ice area amounts to 0.0–1.3 million km^2 (0.0–0.6 million km^2 for extent). The main features of annual and decadal variability are similar in all of them. Thus, all the algorithms show the minima of 1990 (low-frequency algorithms only), 1995 and 2007 as well as the new record of 2012. The results from all the algorithms are highly correlated ($R^2 > 0.9$ for anomalies, Table V(a) and (b).

To give more detailed quantification of the differences among the algorithms, we calculate the ensemble mean, which is the mean sea ice area/extent of all the algorithms, the bias relative to the mean (the difference of the given algorithm from the ensemble mean, averaged over all the years), and the standard deviation of each algorithm from the ensemble mean. This standard deviation (std) is calculated as

$$std = \sqrt{\frac{1}{N-1}\sum_{i=1}^{N}(x_i - \overline{x}_i)^2} \tag{7}$$

where N is a number of years, x_i is an unbiased area or extent for a given algorithm in year i, and $\overline{x}_i$ is the ensemble mean for year i.

The biases (relative to the ensemble mean) and standard deviations are presented in the Table VI(a)–(d) (the two last columns). The most biased algorithms are UMass-AES (1979–2012: 0.625 million km^2 in area and 0.366 million km^2 in extent; 1992–2012: 0.682 million km^2 area and 0.389 million km^2 in extent), NASA Team (1979–2012: -0.703 million km^2 in area and -0.263 million km^2 in extent, and -0.670 million km^2 in area and -0.208 million km^2 in extent for 1992–2012), and Near 90 GHz (-0.219 million km^2 in extent for 1992–2012). The least biased for area were NORSEX (0.203 million km^2 in 1979–2012) and ASI (0.198 million km^2 in 1992–2012), and for extent it was CalVal (-0.044 million km^2 in 1979–2012 and -0.013 million km^2 in 1992–2012). It should be noted that biases are often the same or very close for the long and short periods.

We suggest the biases of the algorithms are, to a large extent, determined by the choice of tie-points (see Table IV for selected tie-points' sets). As an example, we compared the Bristol and NORSEX algorithms that originally use different sets of tie-points. The mean difference in annual sea ice area (1979–2012) between these algorithms amounted to 0.55 million km^2, while running the Bristol algorithm with the tie-points from the NORSEX algorithm reduced this difference to 0.07 million km^2. The change of the tie-point set does not have much influence on the trends (the trend for the Bootstrap algorithm has become 0.02 million km^2 per decade smaller, which amounts to 3.8% of the trend value).

Since bias can eventually be corrected by tie-points adjustment, we do not give it as much weight as the standard deviations. For the period 1979–2012, the largest standard deviation was observed for Bristol (0.059 million km^2 for area and 0.053 million km^2 for extent), and for the period 1992–2012 it was ASI (0.111 million km^2) for area and ASI and Near 90 GHz (both 0.026 million km^2) for extent. The smallest standard deviation was observed for CalVal (0.023 and

TABLE VI
(a) SEA-ICE AREA LINEAR TRENDS IN MILLION km^2/DEC 1979–2012, BIAS AND STD IN MILLION km^2. (b) SEA-ICE AREA LINEAR TRENDS IN MILLION km^2/DEC 1992–2012, BIAS AND STD IN MILLION km^2. (c) SEA-ICE EXTENT LINEAR TRENDS IN MILLION km^2/dec 1979–2012, BIAS AND STD IN MILLION km^2. (d) SEA-ICE EXTENT LINEAR TRENDS IN MILLION km^2/DEC 1992–2012, BIAS AND STD IN MILLION km^2

(a)

Algorithm	September	Annual Mean	March	Bias, annual	Std, annual
Bristol	-0.852	-0.563	-0.374	-0.352	0.059
Cal Val	-0.899	-0.566	-0.370	0.227	0.023
NASA Team	-0.846	-0.563	-0.344	-0.703	0.043
NORSEX	-0.876	-0.573	-0.379	0.203	0.037
UMass-AES	-0.880	-0.534	-0.371	0.625	0.045

(b)

Algorithm	September	Annual Mean	March	Bias, annual	Std, annual
ASI	-1.381	-0.766	-0.387	0.198	0.111
Bootstrap	-1.366	-0.956	-0.557	-0.294	0.068
Bristol	-1.456	-0.966	-0.643	-0.308	0.072
Cal Val	-1.502	-0.923	-0.521	0.265	0.022
NASA Team	-1.290	-0.883	-0.540	-0.670	0.041
NASA Team2	-1.454	-0.978	-0.603	0.244	0.061
Near90GHz	-1.396	-0.808	-0.430	-0.243	0.105
NORSEX	-1.515	-0.975	-0.576	0.241	0.053
NORSEX85H	-1.519	-0.977	-0.575	0.226	0.054
TUD	-1.434	-0.835	-0.468	-0.340	0.049
UMass-AES	-1.489	-0.866	-0.503	0.682	0.037

(c)

Algorithm	September	Annual Mean	March	Bias, annual	Std, annual
Bristol	-0.824	-0.439	-0.305	-0.162	0.053
Cal Val	-0.875	-0.485	-0.372	-0.044	0.020
NASA Team	-0.868	-0.450	-0.333	-0.263	0.033
NORSEX	-0.844	-0.485	-0.383	0.102	0.019
UMass-AES	-0.866	-0.491	-0.395	0.366	0.045

(d)

Algorithm	September	Annual Mean	March	Bias, annual	Std, annual
ASI	-1.496	-0.758	-0.461	-0.143	0.026
Bootstrap	-1.547	-0.794	-0.468	-0.041	0.009
Bristol	-1.507	-0.812	-0.471	-0.093	0.021
Cal Val	-1.544	-0.796	-0.473	-0.013	0.008
NASA Team	-1.511	-0.767	-0.437	-0.208	0.019
NASA Team2	-1.515	-0.796	-0.486	0.172	0.020
Near90GHz	-1.559	-0.779	-0.443	-0.219	0.026
NORSEX	-1.558	-0.806	-0.485	0.134	0.017
NORSEX85H	-1.577	-0.814	-0.486	0.114	0.021
TUD	-1.542	-0.783	-0.458	-0.092	0.014
UMass-AES	-1.533	-0.769	-0.489	0.389	0.021

0.022 million km^2 for area over 1979–2012 and 1992–2012, respectively, and 0.020 and 0.008 million km^2 for extent for the periods 1979–2012 and 1992–2012 respectively), NORSEX (0.019 million km^2 for extent 1979–2012), and Bootstrap (0.009 million km^2 for extent 1992–2012).

We have also calculated standard deviations of all the algorithms from the mean ((8)) for the annual time series (grey lines in Fig. 1). For this purpose, values of all the algorithms for a given year are considered as independent measurements of area or extent for this year

$$std_{\text{all algorithms}}(year) = \pm\sqrt{\frac{1}{N_{\text{alg}}-1}\sum_{\text{alg}=1}^{N_{\text{alg}}}\left(x_{\text{alg}}-\overline{x(year)}\right)^2} \quad (8)$$

where N_{alg} is the number of algorithms, x_{alg} is area or extent in a given year for algorithm 'alg', and $\overline{x(year)}$ is the mean from all the algorithms for a given year. The values of the standard deviations vary from year to year and lie in the range of 0.481–0.559 million km^2 for area 1979–2012, 0.216–0.335 million km^2 for extent 1979–2012, 0.359–0.422 million km^2 for area 1992–2012, and 0.167–0.208 million km^2 for extent 1992–2012. Some of the algorithms lie outside these margins: UMass-AES and NASA Team for area, and UMass-AES for extent (all for both periods).

Standard deviations of area and extent were also calculated for each month [(7) with i being the month and x_i-the detrended area/extent values] and are presented in Fig. 2 for both periods. The standard deviations of the extent are smaller in magnitude than those of area (larger differences are introduced in the area because of its dependence on sea ice concentration).

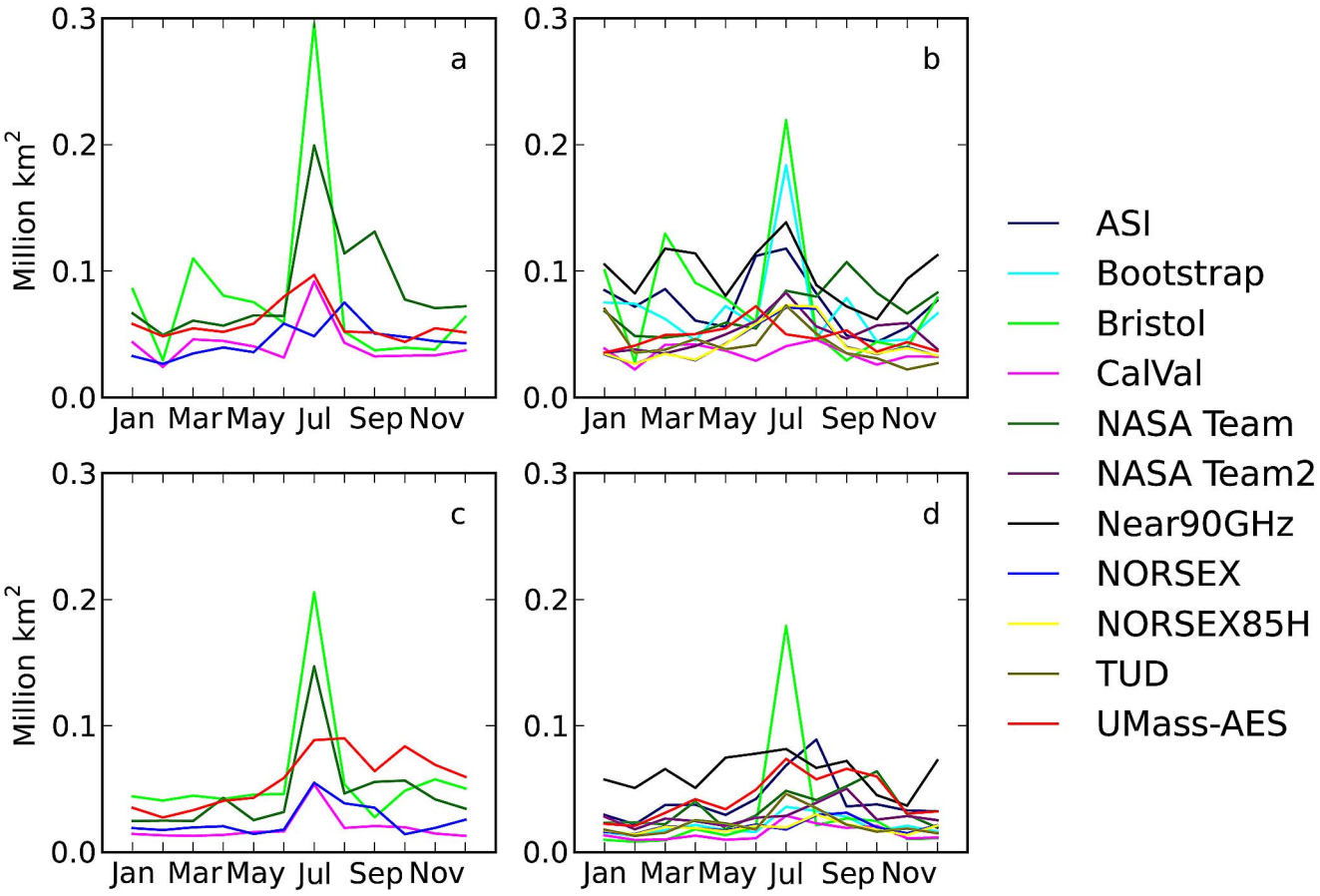

Fig. 2. Standard deviations of area (top row) and extent (bottom row) anomalies for the periods 1979–2012 (left column, five low-frequency algorithms) and 1992–2012 (right column, all the algorithms) for each algorithm from the ensemble mean.

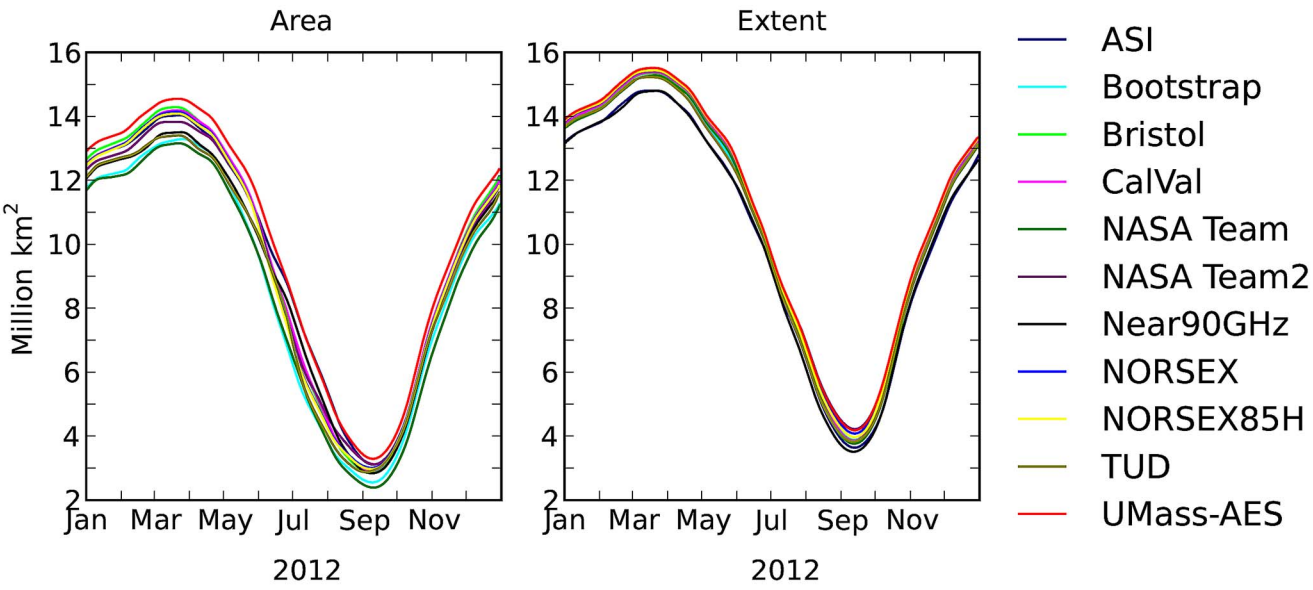

Fig. 3. Daily Arctic sea-ice area (left) and extent (right), 2012, obtained by the 11 algorithms.

The Bristol algorithm stands out with its high standard deviation for July, which is caused by the use of the tie-points from [1]. The latter has a peak for this month in the 19 and 37 GHz channels (Bristol is the only algorithm that uses these tie-points for these channels) for multi-year ice emissivities. The Bootstrap algorithm has a similar peak for the 1992–2012 period (this algorithm is excluded from the analysis of 1979–2012), which is explained by this algorithm also having special tie-points values for July. Finally, the NASA Team algorithm has a peak in July (July–September for area) only for the 1979–2012 time period, but not for 1992–2012. We suggest this can be caused by the fact that this is the only algorithm that uses

different tie-points for SMMR and SSM/I (NORSEX does so only for open water), which might cause more scatter in the data for the two instruments included in the 1979–2012 time series. The surface signatures are more variable at this time of year (mixture of ice and water areas, presence of melt ponds and wet snow/ice, more contribution from the atmosphere), while the tie-points are fixed values, which are not able to capture these changes. Modifying the tie-points to accommodate these surface and atmospheric changes is arguably a possible way to improve the ice concentration calculations, but we could not do this in a systematic way for all algorithms.

To give an impression of day-to-day differences between the algorithms, the daily data for 2012 area and extent are presented in Fig. 3. The difference in daily sea ice area varies between 0.1 and 1.4 million km^2 (the maximal difference occurs in the end of June), while for the extent it varies between 0.1 and 0.7 million km^2 (the maximal difference occurs in the end of May).

V. Sea-Ice Concentration, Spatial Distribution of Differences

The pixel-by-pixel standard deviations from the ensemble mean [(8)] for percentage sea ice concentration obtained by all the algorithms are presented in Fig. 4. March and September are shown for the time periods of 1979–2012 [only the five low-frequency algorithms, Fig. 4(a) and (b)] and 1992–2012 [all 11 algorithms, Fig. 4(c) and (d)]. In winter (March) the largest deviations for both periods amount to 5–12% and are located in the Sea of Okhotsk, and the Bering, Labrador, Greenland, and Barents seas. These areas are characterized by relatively low sea-ice concentrations, and are thus more influenced by atmospheric effects. Since the algorithms have different sensitivity to atmospheric influence, larger differences in the retrievals are observed in these regions. Also, the difference in spatial resolution of the different channels (Table III) plays a larger role here than in regions with less variable sea ice concentration. In the other seas and in the central part of the Arctic, the differences are lower (2.0–2.5% in 1979–2012 and 1.0–1.5% in 1992–2012) because in areas of more consolidated ice the atmosphere is less variable, and differences in spatial resolution play a smaller role. Also, Odden is an area where the standard deviations are low, which may be explained by the fact that Odden did not occur frequently (for March it was present for 17 years out of 32, mostly in the first part of the time period 1979–2012) and there was low/zero concentration often in this region. As for summer (September), the standard deviations are mostly in the range 2–8% and are located everywhere where sea ice is present, reaching values of 12% in the Canadian Archipelago area. This time of year is characterized by the presence of melt-ponds, ice/water mixtures and more atmospheric humidity, which all contribute to the larger differences in the retrievals.

The algorithms tend to deviate from the mean along the coasts in summer and in the more southern seas in winter. Despite the land-ocean spillover mask being applied, the land contamination was not completely removed. Disagreement of the algorithms in these areas is believed to be a consequence of combined effect of differences in footprint size in the channels and the calculation schemes in the algorithms.

VI. Linear Trends

A. Area and Extent: Annual Minimum, Mean, and Maximum

To estimate Arctic sea-ice area and extent change during the 34- and 21-year periods, linear trends were calculated for annual mean, minimum (September) and maximum (March) sea-ice. The trends represent change in sea-ice area and extent in million km^2 per decade from 1979 to 2012 [Table VI(a) and (c)] and from 1992 to 2012 [Table VI(b) and (d)].

According to five low-frequency algorithms, annual Arctic sea-ice area decreased from 1979 to 2012 at the rate of 0.534–0.573 million km^2 per decade (0.439–0.491 million km^2 per decade for extent), and the decrease amounted to 0.866–0.975 million km^2 per decade (0.767–0.812 million km^2 per decade for extent) for the 1992–2012 period. All the algorithms show the accelerated decrease in sea-ice in the second period in comparison to the earlier years. The processes driving this acceleration are explained in detail in [40]. For the high-frequency algorithms (1992–2010) the area decrease amounted to 0.766–0.978 million km^2 per decade (0.758–0.814 million km^2 per decade for extent), which shows slightly larger spread than for the low-frequency algorithms. Linear trends for the ensemble means were also calculated (dark red lines in Fig. 1). The 1979–2012 trend in area amounted to -0.560 million km^2 per decade and -0.470 million km^2 per decade for extent, while the area trend for 1992–2012 was -0.903 million km^2 per decade, and -0.789 million km^2 per decade for extent.

To compare with previously published trend values we calculated the mean extent trend for the period of 1979–2010, which gave -0.422 million km^2 per decade, while [10] retrieved -0.515 million km^2 per decade and [16] retrieved -0.469 million km^2 per decade (November 1978–December 2010). [14] obtained the extent trend for November 1978–December 2007 of -0.387 to -0.466 million km^2 per decade, depending on the instrument used and whether the adjustments between the instruments have been applied. Our mean trend (1979–2007) was -0.376 million km^2 per decade, being lower than those of [14]. However, [14] showed that applying the instrument adjustments changed the trend from -0.466 million km^2 per decade (no adjustment) to -0.387 million km^2 per decade (after adjustment) for the time series of SMMR-SSM/I-AMSR. Their value for non-adjusted SMMR-SSM/I time series (the one that we use) was -0.397 million km^2 per decade. [3] obtained a trend in the extent of -0.327 million km^2 per decade (Bristol) and -0.317 million km^2 per decade (NASA Team) for the period of 1987–2004, while our value of mean trend was -0.370 million km^2 per decade. Their values of extent trends for 1991–2004 were from -0.419 to -0.478 million km^2 per decade (Bristol, NASA Team, NASA Team2, Near 90 GHz, and TUD), while our value was -0.494 million km^2 per decade (1992–2004). Unconstrained versions of the algorithms (allowing sea ice concentrations below 0% and above 100%) were used in [3], while our versions are constrained, which might have contributed to the differences in obtained trends.

Sea-ice decline in summer contributes much more to the annual average decline than does the winter decline [Table VI(a)–(d)]. According to the low-frequency algorithms, September (annual minimum) average ice area has declined at a

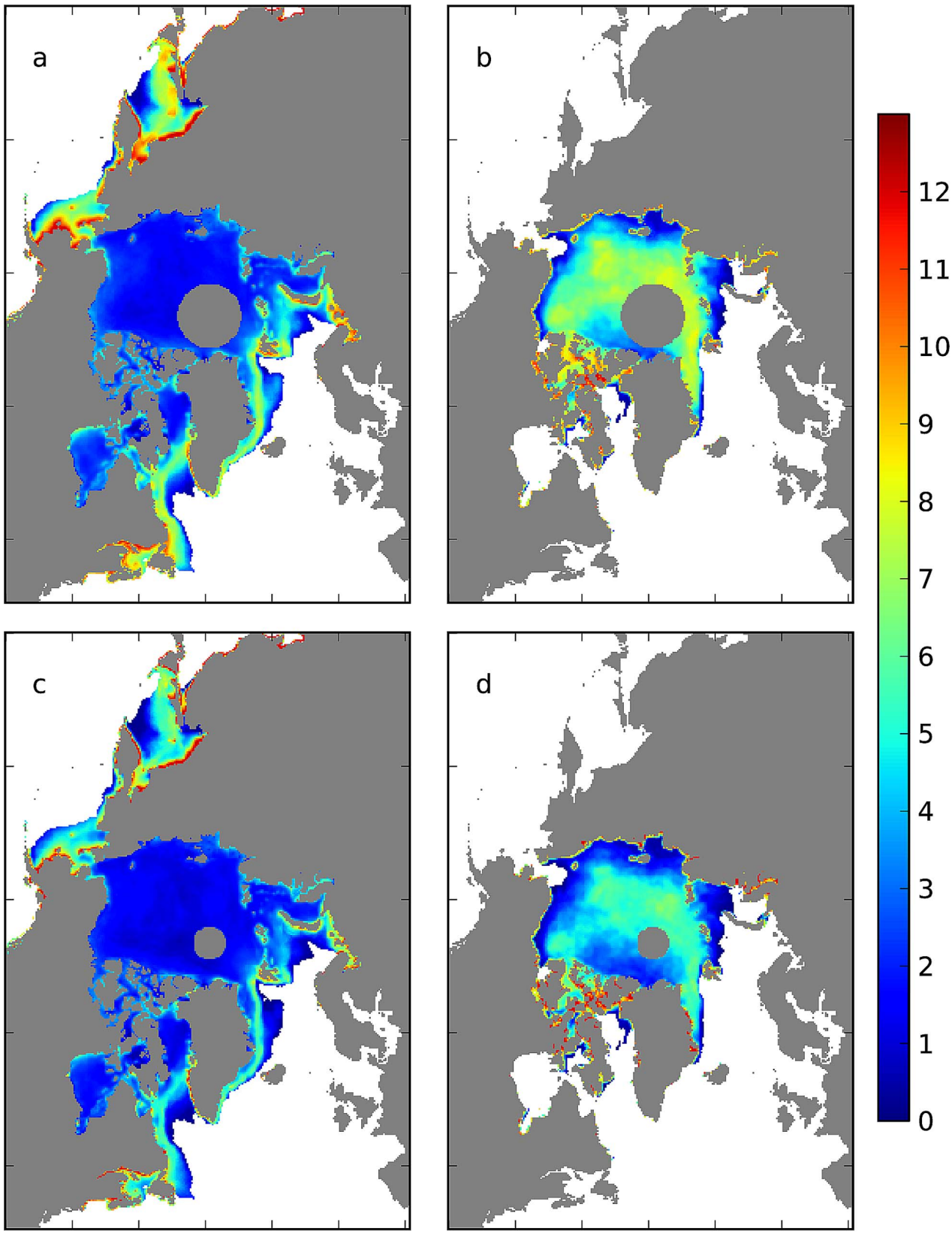

Fig. 4. Sea-ice concentration: standard deviation of all the algorithms from the ensemble mean, %. (a), (b) 1979–2012 March and September, respectively, 5 algorithms (Bootstrap is not included). (c), (d) 1992–2012 March and September, respectively, 11 algorithms.

rate of 0.846–0.899 million km^2 (0.824–0.875 million km^2 for extent) per decade (1979–2012) while March (annual maximum) ice area has declined with a rate of 0.344–0.379 million km^2 (0.305–0.395 million km^2 for extent) per decade (1979–2012). For the period 1992–2010, the September sea-ice area decrease amounted to 1.290–1.515 million km^2 (1.507–1.558 million km^2

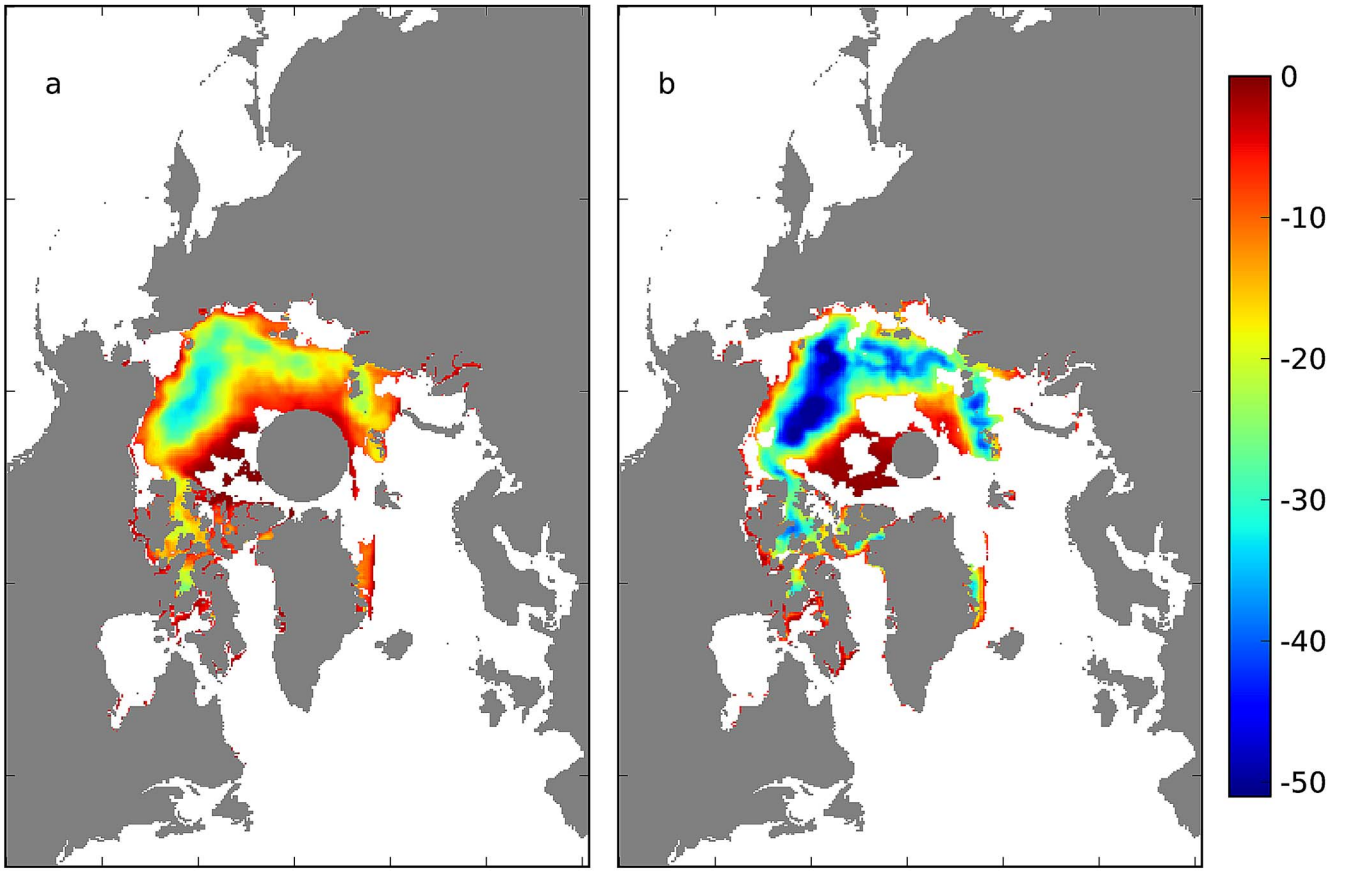

Fig. 5. Linear trends (statistically significant at 95%) in sea-ice concentration in September in % per decade for the period 1979–2012 [(a) average of five algorithms] and 1992–2012 [(b) average of 11 algorithms].

for extent) per decade for the low-frequency algorithms and to 1.381–1.519 million km^2 (1.496–1.577 million km^2 for extent) for the high-frequency algorithms. The sea-ice area decrease in March amounted to 0.503–0.643 million km^2 (0.437–0.489 million km^2 for extent) per decade for the low-frequency algorithms and to 0.387–0.603 million km^2 (0.443–0.486 million km^2 for extent) for the high-frequency algorithms.

The trends for the area were found to be larger than for the extent, which is caused by negative trends in the sea-ice concentrations (see the next paragraph) that are used to calculate the area.

B. Sea-Ice Concentration

Sea-ice concentration trends were assessed as a change in percentage sea-ice concentration per decade from 1979 to 2012 for low-frequency algorithms and from 1992 to 2012 for all the algorithms. The trends were calculated for the month of sea ice annual minimum (average September), the annual mean and the annual maximum (average March). The trends in winter were very small (0 to −5% per decade), whereas the summer (September) trends (shown in Fig. 5) contributed the most to the annual sea-ice decline. The summer trends were negative in all regions of the Arctic except a relatively small area around Svalbard where trend values were positive, but not significant (at 95% level). Fig. 5 only shows trends that are statistically significant at the 95% confidence interval, and these are always negative.

Summer sea-ice concentration has changed at different rates in different areas of the Arctic. As seen from Fig. 5, the trends in the vicinity of the no-data circle at the Pole and the area north of the Canadian Archipelago are zero. These are areas with the thickest and oldest sea ice and where ice still persists throughout the year. For both the 21-year and 34-year periods the summer decrease was most pronounced in the area of the East Siberian and Beaufort seas (−5 to −30% in 1979–2012 and −5 to −50% in 1992–2012), the next largest trends were observed in the area of the northern Laptev, Kara and Barents seas (−10 to −20% in 1979–2012 and −10 to −40% in 1992–2012)), followed by the western Greenland Sea (−10% in 1979–2012 and −5 to −20 in 1992–2012). The areas where the trends over 1992–2012 reach up to around −50% per decade are the areas where September sea ice has disappeared (the concentration has decreased by 100%, which gives about −50% per decade for 21 years) during this period. Accordingly, the summer trend in these areas for 1979–2012 is about −30%.

VII. Discussion and Conclusions

Absolute values of annual Arctic sea ice area and extent differ substantially between the investigated algorithms (up to 1.3 million km^2 per decade for area and up to 0.6 million km^2

per decade for extent), but they all agree on the trends in both area and extent within 0.05 million km^2 per decade (1979–2012, five algorithms) and 0.21 million km^2 per decade (1992–2012, 11 algorithms).

The absolute differences among sea ice algorithms can be caused by different choice and utilization of the channels, tie-points, sensitivities to changes in physical temperature of the emitting layer and weather filters [13]. To minimize the differences due to factors not directly related to the algorithms basics, we use the same weather filter, open-ocean and land-ocean spillover masks, and surface temperature (in the algorithms that require it) in all the algorithms. These settings may not be the same as in other published results but allows us a more direct comparison of the algorithms themselves.

We found that algorithms using similar channels form two groups, where the correlation between the algorithms in the same group is higher than otherwise [Table V(a) and (b)]: 1. UMass-AES, NORSEX, CalVal, and Bristol (they all use 19 V and 37 V channels), and 2. ASI, TUD, Near 90 GHz and NORSEX85H (as algorithms using higher frequencies). The choice of channels implies a variety of different effects. As described in [4] the snow and ice layering and the presence of thin ice influence horizontally polarized channels most, while coarse snow grains, and therefore larger volume scattering, affect the spectral gradient rather than polarization. Microwave frequency (or wavelength) is also an important factor because of different penetration depth at different frequencies/wavelengths. The penetration is deeper at lower frequencies meaning these algorithms respond less to snow variations, whereas for the high frequency algorithms, penetration reaches only a little more than typical snow depths (10–20 cm) and so these algorithms are more sensitive to snow variability. In addition, sensor footprint is different in each channel (Table III), which may have an effect on sea ice area and extent retrievals by the algorithms. To evaluate each of these effects is a large and complex task in itself and will require a large volume of reliable in situ data and/or reliable snow/ice emissivity models to succeed.

We were not able to conclude whether usage of polarization or gradient ratio, radiative transfer model approach or surface air temperature had an effect on the magnitude of the differences between the algorithms. It appears that all these factors influence the differences in a complicated and interdependent way and that these connections will need further investigation of the interaction of the microwave emission with the surfaces and atmosphere under different conditions to fully resolve the impact.

Based on our analysis, we conclude that the algorithms obtain similar variability in sea ice to a large extent, but are individually biased from the mean, which is mainly due to different choice of tie-points. Because tie-points are generally the constant coefficients of the algorithms, their adjustments can lead to a better agreement in the sea-ice absolute values obtained by the different algorithms. In addition, our analysis shows that the algorithms deviations from the ensemble mean are correlated with seasonal emissivity variations, which means proper selection of seasonal tie-points is very important.

According to the five low-frequency algorithms, average Arctic sea-ice area decreased at the rate of 0.534–0.573 million km^2 per decade (0.439–0.491 million km^2 per decade for extent) from 1979 to 2010, and 0.866–0.975 million km^2 per decade (0.767–0.812 million km^2 per decade for extent) for 1992–2010 period. The trends for the latter period were larger, which shows the sea-ice decline acceleration confirmed by all the algorithms. The analogous trends were calculated for the high-frequency algorithms, which cover only the period of 1992–2010, the area decrease amounted to 0.766–0.978 million km^2 per decade (0.758–0.814 million km^2 per decade for extent). All the algorithms agreed in showing much larger sea-ice area and extent decline in September than in March. For both 1979–2012 and 1992–2012 periods, the sea ice decreased most in the East Siberian and Beaufort seas, the northern Laptev, Kara and Barents seas, as well as the western Greenland Sea. The algorithms show a good agreement in the derived trends. The ensemble mean annual sea-ice area decreased by 0.560 million km^2 per decade (0.470 million km^2 per decade for extent) during 1979–2012 (5 algorithms), and by 0.903 million km^2 per decade (0.789 million km^2 per decade for extent) during 1992–2012 (11 algorithms).

The deviations of the algorithms from the ensemble mean vary for area from 0.481 to 0.559 million km^2 (0.216–0.335 million km^2 for extent) during 1979–2012, and from 0.359 to 0.422 million km^2 (0.167–0.208 million km^2 for extent) during 1992–2012. In winter, the algorithms differ most in the Sea of Okhotsk, and the Bering, Labrador, Greenland and Barents seas. This we explain by the proximity of larger areas of open water in these regions, which increases the atmospheric effects and thus increases the algorithms uncertainties. The differences are higher in summer than in winter and are present everywhere where sea ice is present. During summer the retrieval of sea ice properties is complicated because of the wet snow, melt-ponds, and thin ice and water mixtures, which make the retrievals less reliable and the selection of channels in the individual algorithm becomes more important since different channels have different sensitivities to these variations.

Both the trend values and the deviations were larger for area than for extent due to larger direct influence of the individual concentrations on area.

From our analysis we cannot establish an absolute ranking of the performance of the algorithms because of the lack of good validation data. In parallel with what is done with the different output from coupled climate simulation data, where the ensemble of the different models is calculated, it may be recommendable to do a similar ensemble calculation for all the different passive microwave sea ice concentration algorithms.

ACKNOWLEDGMENT

The authors thank the National Snow and Ice Data Center, University of Colorado, Boulder, USA (NSIDC) for providing the brightness temperature input data and assistance, S. Tressel, Professional Research Assistant at NSIDC, R. Davy, Nansen Environmental and Remote Sensing Center, Bergen, Norway (NERSC) and M. Miles, Uni Research, Bergen, Norway for their assistance; Dr. T. Markus, NASA Goddard Space Flight Center, Greenbelt, USA, and K. Kloster, NERSC for providing codes of the NASA Team2 and NORSEX-85H algorithms, respectively, as well as helping with good advices.

REFERENCES

[1] S. Andersen, "Monthly arctic sea ice signatures for use in passive microwave algorithms," Danish Meteorological Institute, Copenhagen, Denmark, Tech. Rep. 98-18, 1998.

[2] S. Andersen, R. Tonboe, S. Kern, and H. Schyberg, "Improved retrieval of sea ice total concentration from spaceborne passive microwave observations using numerical weather prediction model fields: An intercomparison of nine algorithms," *Remote Sens. Environ.*, vol. 104, no. 4, pp. 374–392, Oct. 2006.

[3] S. Andersen, R. T. Tonboe, and L. Kaleschke, "Satellite thermal microwave sea ice concentration algorithm comparison," in *Arctic Sea Ice Thickness: Past, Present, and Future. Climate Change and Natural Hazards Series*, vol. 10, P. Wadhams and G. Amanatidis, Eds. Brussels, Belgium: European Commission, 2007, EUR 22416.

[4] S. Andersen, R. T. Tonboe, L. Kaleschke, G. Heygster, and L. T. Pedersen, "Intercomparison of passive microwave sea ice concentration retrievals over the high-concentration Arctic sea ice," *J. Geophys. Res.*, vol. 112, no. C8, pp. C08004-1–C08004-18, Aug. 2007.

[5] Arctic Regional Ocean Observing System (Arctic ROOS). [Online]. Available: http://arctic-roos.org/observations/comparison-of-algorithms

[6] E. Bjørgo, O. M. Johannessen, and M. W. Miles, "Analysis of merged SMMR-SSMI time series of Arctic and Antarctic sea ice parameters 1978–1995," *Geophys. Res. Lett.*, vol. 24, no. 4, pp. 413–416, Feb. 1997.

[7] D. J. Cavalieri, P. Gloersen, and W. J. Campbell, "Determination of sea ice parameters with the NIMBUS 7 SMMR," *J. Geophys. Res.*, vol. 89, no. D4, pp. 5355–5369, Jun. 1984.

[8] D. J. Cavalieri, K. S. Germain, and C. T. Swift, "Reduction of weather effects in the calculation of sea ice concentration with the DMSP SSM/I," *J. Glaciol.*, vol. 41, no. 139, pp. 455–464, 1995.

[9] D. J. Cavalieri, C. L. Parkinson, P. Gloersen, and H. J. Zwally, *Arctic and Antarctic Sea Ice Concentrations from Multichannel Passive-Microwave Satellite Data Sets: October 1978–September 1995*. Greenbelt, MD, USA: Goddard Space Flight Center, 1997, p. 17, User's Guide—NASA TM 104647.

[10] D. J. Cavalieri and C. L. Parkinson, "Arctic sea ice variability and trends, 1979–2010," *Cryosphere*, vol. 6, pp. 881–889, 2012.

[11] J. C. Comiso, "Characteristics of arctic winter sea ice from satellite multispectral microwave observations," *J. Geophys. Res.*, vol. 91, no. C1, pp. 975–994, Jan. 1986.

[12] J. C. Comiso and C. W. Sullivan, "Satellite microwave and *in situ* observations of the Weddell Sea ice cover and its marginal ice zone," *J. Geophys. Res.*, vol. 91, no. C8, pp. 9663–9681, Aug. 1986.

[13] J. C. Comiso, D. J. Cavalieri, C. L. Parkinson, and P. Gloersen, "Passive microwave algorithms for sea ice concentration: A comparison of two techniques," *Remote Sens. Environ.*, vol. 60, no. 3, pp. 357–384, Jun. 1997.

[14] J. C. Comiso and F. Nishio, "Trends in the sea ice cover using enhanced and compatible AMSR-E, SSM/I, and SMMR data," *J. Geophys. Res.*, vol. 113, no. C2, pp. C02S07-1–C02S07-22, Feb. 2008.

[15] J. C. Comiso and C. L. Parkinson, "Arctic sea ice parameters from AMSR-E data using two techniques and comparisons with sea ice from SSM/I," *J. Geophys. Res.*, vol. 113, no. C2, pp. C02S05-1–C02S05-16, Feb. 2008.

[16] J. C. Comiso, "Large decadal decline of the Arctic multiyear ice cover," *J. Climate*, vol. 25, no. 4, pp. 1176–1193, Feb. 2012.

[17] W. J. Emery, C. Fowler, and J. Maslanik, "Arctic sea ice concentrations from special sensor microwave imager and advanced very high resolution radiometer satellite data," *J. Geophys. Res.*, vol. 99, no. C9, pp. 18 329–18 342, Sep. 1994.

[18] P. Gloersen, W. J. Campbell, D. J. Cavalieri, J. C. Comiso, C. L. Parkinson, and H. J. Zwally, *Arctic and Antarctic Sea Ice, 1978–1987: Satellite Passive Microwave Observations*. Washington DC, USA: NASA, 1991.

[19] P. Gloersen and D. J. Cavalieri, "Reduction of weather effects in the calculation of sea ice concentration from microwave radiances," *J. Geophys. Res.*, vol. 91, no. C3, pp. 3913–3919, Mar. 1986.

[20] O. M. Johannessen and N. Ivanova, "Sea ice passive microwave algorithms and SAR validation," presented at the ESA Living Planet Symp., Bergen, Norway, Jun. 28–Jul. 2, 2010, SP-686.

[21] L. Kaleschke, C. Lupkes, T. Vihma, J. Haarpaintner, A. Bochert, J. Hartmann, and G. Heygster, "SSM/I sea ice remote sensing for mesoscale ocean-atmosphere interaction analysis," *Can. J. Remote Sens.*, vol. 27, no. 5, pp. 526–537, 2001.

[22] V. M. Kattsov, V. E. Ryabinin, J. E. Overland, M. C. Serreze, M. Visbeck, J. E. Walsh, W. Meier, and X. Zhang, "Arctic sea-ice change: A grand challenge of climate science," *J. Glaciol.*, vol. 56, p. 200, Dec. 2010.

[23] S. Kern and G. Heygster, "Sea-ice concentration retrieval in the Antarctic based on the SSM/I 85.5 polarization," *Ann. Glaciol.*, vol. 33, no. 1, pp. 109–114, Jan. 2001.

[24] S. Kern and L. Kaleschke, "Two ice concentration algorithms benefitting from 85 GHz special sensor microwave/imager data: A comparison," in *Proc. IEEE Int. Geosci. Remote Sens. Symp.*, 2002, pp. 1938–1940.

[25] K. Kloster, "Ice type concentration by microwave radiometry," Norwegian Space Center, Oslo, Norway, Earth Observation Compendium for Course AGF-207, 1996.

[26] C. Kongoli, S. A. Boukabara, Y. F. W. Banghua, and R. A. Ferraro, "New sea-ice concentration algorithm based on microwave surface emissivities—Application to AMSU measurements," *IEEE Trans. Geosci. Remote Sens.*, vol. 49, no. 1, pp. 175–189, Jan. 2011.

[27] R. Kwok and N. Untersteiner, "The thinning of Arctic sea ice," *Phys. Today*, vol. 64, no. 4, pp. 36–41, Apr. 2011.

[28] T. Markus and D. J. Cavalieri, "An enhancement of the NASA Team sea ice algorithm," *IEEE Trans. Geosci. Remote Sens.*, vol. 38, no. 3, pp. 1387–1398, 2000.

[29] J. Maslanik and J. Stroeve, "DMSP SSM/I-SSMIS daily polar gridded brightness temperatures, Version 4," NASA DAAC, Nat. Snow Ice Data Center, Boulder, CO, USA, 2012.

[30] C. Melsheimer, G. Heygster, and L. T. Pedersen, "Retrieval of sea ice emissivity and integrated retrieval of surface and atmospheric parameters over the Arctic from AMSR-E data," *J. Remote Sens. Soc. Jpn.*, vol. 29, no. 1, pp. 236–241, 2009.

[31] NASA Goddard Space Flight Center, NASA GSFC. CD-ROM, NIMBUS-7 SMMR Brightness Temperature Grids for the Northern Hemisphere, 25.10.1978–31.07.1987, Greenbelt, MD, USA.

[32] L. T. Pedersen, "Improved spatial resolution of SSM/I products. Development of new satellite ice data products," Nansen Environ. Remote Sens. Center, Bergen, Norway, 1998, Tech. Report.

[33] R. O. Ramseier, I. G. Rubinstein, and A. F. Davies, "Operational evaluation of special sensor microwave/imager by the atmospheric environment service," Centre Res. Exp. Space Sci., York Univ., North York, ON, Canada, 1988.

[34] R. O. Ramseier, "Sea ice validation," in *DMSP Special Sensor Microwave/Imager Calibration/Validation*, J. P. Hollinger, Ed. Washington, DC, USA: Naval Research Laboratory, 1991.

[35] M. Shokr, A. Lambe, and T. Agnew, "A new algorithm (ECICE) to estimate ice concentration from remote sensing observations: An application to 85-GHz passive microwave data," *IEEE Trans. Geosci. Remote Sens.*, vol. 46, no. 12, pp. 4104–4121, Dec. 2008.

[36] D. M. Smith, "Extraction of winter total sea-ice concentration in the Greenland and Barents Seas from SSM/I data," *Int. J. Remote Sens.*, vol. 17, no. 13, pp. 2625–2646, Sep. 1996.

[37] D. M. Smith and E. C. Barrett, "Satellite mapping and monitoring of sea ice," Defense Res. Agency, RSU, Univ. Bristol, Bristol, U.K., 1994.

[38] G. L. Spreen, L. Kaleschke, and G. Heygster, "Sea ice remote sensing using AMSR-E 89-GHz channels," *J. Geophys. Res.*, vol. 113, no. C2, pp. C02S03-1–C02S03-14, Feb. 2008.

[39] K. Steffen, D. J. Cavalieri, J. C. Comiso, K. St. Germain, P. Gloersen, and I. Rubinstein, "The estimation of geophysical parameters using passive microwave algorithms," in *Microwave Remote Sensing of Sea Ice*, F. Carsey, Ed. Washington, DC, USA: American Geophysical Union, 1992, pp. 201–231.

[40] J. C. Stroeve, M. C. Serreze, M. M. Holland, J. E. Kay, J. Malanik, and A. P. Barrett, "The Arctic's rapidly shrinking sea ice cover: A research synthesis," *Clim. Change*, vol. 110, no. 3/4, pp. 1005–1027, Feb. 2012.

[41] E. Svendsen, K. Kloster, B. Farrelly, O. M. Johannessen, J. A. Johannessen, W. J. Campbell, P. Gloersen, D. Cavalieri, and C. Matzler, "Norwegian remote sensing experiment' evaluation of the nimbus 7 scanning multichannel microwave radiometer for sea ice research," *J. Geophys. Res.*, vol. 88, no. C5, pp. 2781–2791, Mar. 1983.

[42] E. Svendsen, C. Matzler, and T. Grenfell, "A model for retrieving total sea ice concentration from a spaceborne dual-polarized passive microwave instrument operating near 90 GHz," *Int. J. Remote Sens.*, vol. 8, no. 10, pp. 1479–1487, Oct. 1987.

[43] C. Swift, L. Fedor, and R. O. Ramseier, "An algorithm to measure sea ice concentration with microwave radiometers," *J. Geophys. Res.*, vol. 90, no. C1, pp. 1087–1099, Jan. 1985.

[44] J. M. Walters, C. Ruf, and C. T. Swift, "A microwave radiometer weather-correcting sea ice algorithm," *J. Geophys. Res.*, vol. 92, no. C6, pp. 6521–6534, Jun. 1987.

Natalia Ivanova received the Ph.D. degree in physical oceanography in 2008 from Russian State Hydrometeorological University, Saint-Petersburg, Russia.

During her Ph.D., she worked at the Nansen International Environmental and Remote Sensing Center in Saint-Petersburg, Russia, from 2004 to 2007 and at the Nansen Environmental and Remote Sensing Center in Bergen, Norway from 2007 to 2008. Her Ph.D. work was related to satellite radar imaging of sea surface contaminations, which involved semi-analytical model investigations and several applications. Since 2008, she works as a Post-Doc at Nansen Environmental and Remote Sensing Center in Bergen. Her research interests include satellite remote sensing of sea ice. Currently, she works with passive microwave data utilization for Arctic sea ice retrievals.

Ola M. Johannessen received the degree Cand. Real. in physical oceanography from University of Bergen, Norway, in 1965. In 1987 he became a professor in the Geophysical Institute, University of Bergen.

At present, he is a Senior Scientist and Nansen Fellow at the Nansen Environmental and Remote Sensing Center (NERSC), the Leader of the Nansen Group which consists of six Nansen Centers in Norway, Russia, India, China, South Africa, Bangladesh, the President of Nansen Scientific Society and Visiting Professor at the Institute of Atmospheric Physics at the Chinese Academy of Sciences. He is presently involved in the following scientific fields: Arctic climate system, including sea ice and Greenland ice sheet variability, climate teleconnection between low and high latitude and visa versa. He is also the leader of the Research Council of Norway (RCN), Arctic Sea Ice Variability: a comprehensive study using satellite and in situ observations (ArcticSIV), the RCN Decadal to multidecadal variability in the Indian Monsoon Rainfall and teleconnection with Atlantic Multidecadal oscillation (India-Clim) and the Mohn-Sverdrup Norwegian Sea and Greenland Ice Sheet projects. He is the author and coauthor of more than 500 publications of which nine are books and 144 are in referee journals. At present he is Council member of the Global Climate Forum (GCF), member of the editorial board of PRAXIS Publishing Ltd and Co-Chief editor of the journal *Atmospheric and Oceanic Science Letter* of the Chinese Academy of Science and member of the Editorial Board of the *American Journal of Climate Change*.

Dr. Johannessen has received nine awards for his research and leadership. He was the Laureate of the EU Descartes Prize in Earth Science in 2005 for leading the project "Climate and Environmental Change in the Arctic (CECA)." He received the Fridtjof Nansen Medal for Outstanding Research in 2007. Furthermore, His Majesty King Harald V of Norway appointed him to the Royal Norwegian St. Olavs decoration, Knight of First Class, November 24, 2008. In 2010 he was awarded the honorary membership from the Norwegian Academy of Technological Sciences, (NTVA) and received the "Certificate" from the Director-General of the European Space Agency for his contribution to the "High-Level Science Policy Advisory Committee from 2007–2010." In 2011 he received "The Norwegian Space Center award for his scientific contribution to increase international awareness and understanding of space activities—in particular for Earth observations." He is elected full member of the International Academy of Astronautics, the European Academy of Science and Arts, Finnish Academy of Science and Letters, the Norwegian Academy of Technical Sciences and the Norwegian Academy of Science and Letters and the Norwegian Scientific Academy for Polar Research where he was the President in the period 2008–2012.

Leif Toudal Pedersen (M'82) was born in Denmark in 1957. He received the M.S. degree in microwave engineering from the Technical University of Denmark (TUD), Kongens Lyngby, Denmark, in 1982, and the Ph.D. degree in passive microwave remote sensing of sea ice from the Technical University of Denmark in 1992.

From 1982 to 2000, he was a Research Assistant at the Electromagnetics Institute at TUD and from 2000 to 2007 he was an Associate Professor at Ørsted-DTU, Denmark. Since 2007 he has been a Senior Researcher at the Center for Ocean and Ice at the Danish Meteorological Institute, Copenhagen, Germany. His research interests include the retrieval of ice, ocean and atmospheric parameters from multispectral microwave radiometer measurements as well as other methods for remote sensing of sea ice.

Dr. Pedersen is a member of the Danish National Committee for Climate Research and the Danish National Committee for SCAR. He also serves as a Danish delegate to ESA's Programme Board for Earth Observations and on ESA's Sentinel-1 Mission Advisory Group.

Rasmus T. Tonboe received the M.Sc. degree in geology from the University of Aarhus, Aarhus, Denmark, in 1997 and the Ph.D. degree in geophysics from the University of Copenhagen, Copenhagen, Denmark, in 2004.

Since 1997 he was with the Ice and Remote Sensing Division, the Danish Meteorological Institute, Copenhagen, Germany. From 2006 he was with the Center for Ocean and Ice, Danish Meteorological Institute. He has participated several international research projects and he is the local manager of EUMETSAT's OSI SAF project. His research interests include microwave and infrared remote sensing of sea ice in particular modeling of thermal emission and backscatter from sea ice. He has participated both fieldwork and research cruises in the Arctic.